Sensors and Actuators B 238 (2017) 928–937

Contents lists available at ScienceDirect

Sensors and Actuators B: Chemical

journal homepage: www.elsevier.com/locate/snb

Sub-ppm YSZ-based mixed potential type acetone sensor utilizing columbite type composite oxide sensing electrode

Fangmeng Liu, Bin Wang, Xue Yang, Xishuang Liang*, Peng Sun, Xiaohong Chuai, Yuan Gao, Fengmin Liu, Geyu Lu*

State Key Laboratory on Integrated Optoelectronics, College of Electronic Science and Engineering, Jilin University, 2699 Qianjin Street, Changchun 130012, China

ARTICLE INFO

Article history:
Received 8 April 2016
Received in revised form 8 June 2016
Accepted 30 June 2016
Available online 1 July 2016

Keywords:
Acetone sensor
YSZ
Mixed potential
$CdNb_2O_6$

ABSTRACT

Mixed potential type solid-state electrochemical gas sensors using yttria- stabilized zirconia (YSZ) and columbite composite oxide sensing electrodes (SEs) prepared via a facile sol-gel method were developed for detection of sub-ppm acetone at 600 °C. In the comparison of different devices, the sensor attached with $CdNb_2O_6$-SE displayed the highest response of −25 mV to 5 ppm acetone and even could achieve low detection limit of 200 ppb at 600 °C. The fabricated sensor using $CdNb_2O_6$-SE exhibited rapid response and recovery times to 2 ppm acetone at 600 °C, which are 9 and 21 s, respectively. Additionally, the present device also showed good repeatability, selectivity, wet-resistance and stability in 30 day measured periods at 600 °C. Moreover, the sensing mechanism related to mixed potential was proposed and analyzed quantitatively and further demonstrated by polarization curve.

1. Introduction

Diabetes is common endocrine metabolic disease which accompanies disorder of glycometabolism. It is the third leading cause of death in industrial countries and the number of diabetes patients is continually increasing all over the world [1,2]. Therefore, the early diagnosis of diabetes is very important for the human health. The clinical medicine indicates acetone can be generated via the fatty acid oxidation in diabetes and ketoacidosis lack of insulin. Excessive acetone circulating in the blood system is excreted from the lungs and the concentration in exhaled breath varies from 0.3–0.9 ppm for healthy people and more than 1.8 ppm can be detected for diabetics [3–5]. Hence, acetone has been used as diabetic-specific biomarker for non-invasive early detection or monitoring from exhaled breath. Among the various acetone gas detection methods, development and fabrication of reliable gas sensor with portability, excellent sensing characteristics and low fabrication cost used for real time monitoring acetone gas has attracted more and more attention.

In the past two decades, mixed potential type solid-state electrochemical gas sensor based on yttria-stabilized zirconia (YSZ) electrolyte and metal oxide sensing electrode has been designed and developed widely, aiming at achieving in-situ gas sensing detection [6–11]. According to mixed potential type sensing mechanism proposed by several research groups [12–17], the sensing signal (V) is generated at triple phase boundary (TPB) of sensing electrode, target gas and electrolyte by the electrochemical reaction of anodic and cathodic reactions. The sensing performance is mainly determined by electrochemical catalytic activity of sensing electrode material to target gas. Thus, exploiting and hunting for a suitable SE material is of great importance in developing high performance YSZ-based acetone sensor. Quite recently, we have reported that the use of composite oxide, such as $Zn_3V_2O_8$ [18] and $NiNb_2O_6$ [19], as an SE material for YSZ-bsed mixed potential sensor resulted in high sensitivity in the relative high concentration range and low detection limit of 1 and 0.5 ppm to acetone, respectively. From the practical point of view, the development of acetone sensor with enhanced sensing characteristics in low detection limit, high sensitivity in the low concentration range and good stability is still one of challenging targets.

In the present study, a serious of MNb_2O_6 (M: Cd, Co, Zn, Mn and Ni) columbite type composite oxide materials prepared by a facile sol-gel method were used as sensing electrode for mixed potential type YSZ-based gas sensors, aiming at highly sensitive detection of acetone in the low concentration range suitable for the diabetes monitoring. Among the SEs examined, the sensor attached with $CdNb_2O_6$-SE displayed the largest sensitivity to acetone and the corresponding sensing characteristics including response and

* Corresponding authors.
E-mail addresses: liangxs@jlu.edu.cn (X. Liang), lugy@jlu.edu.cn (G. Lu).

http://dx.doi.org/10.1016/j.snb.2016.06.171
0925-4005/

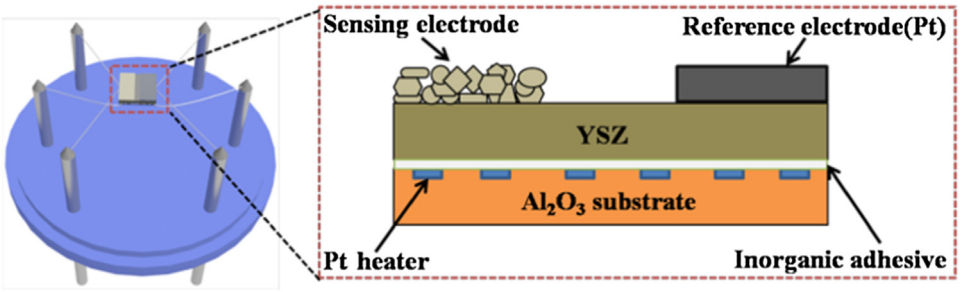

Fig. 1. Schematic diagram of fabricated sensor.

recovery times, selectivity, repeatability, moisture influence and stability were systematically investigated. Besides, as far as we know, this is first study to report the sensor utilizing YSZ and $CdNb_2O_6$-SE for detection of sub-ppm acetone.

2. Experimental

2.1. Preparation and characterization of columbite composite oxide materials

The $CdNb_2O_6$ was synthesized via a sol–gel method from Cadmium nitrate tetrahydrate ($Cd(NO_3)_2{\cdot}4H_2O$), Niobium oxide (Nb_2O_5), HF acid (40%), Ammonium hydroxide ($NH_3{\cdot}H_2O$), Citric acid (CA), and Ammonium nitrate (NH_4NO_3). All of reagents were of analytical grade without further purification. In a typical synthesis process, 3 mmol Nb_2O_5 was dissolved in a certain amount of HF acid after heating in water bath of 80 °C. Then, ammonia hydroxide solution was dropwise added to the above solution until the pH value was up to 9 to obtain $Nb_2O_5{\cdot}nH_2O$ precipitate under stirring constantly. The precipitate was filtered, washed, and dissolved in citric acid aqueous solution and stirred at 80 °C for 2 h. Then, the stoichiometric $Cd(NO_3)_2{\cdot}4H_2O$ and NH_4NO_3 (the molar ratio of $Cd/Nb/NH_4NO_3$ = 1:2:12) were added into the solution described above and then stirred at 80 °C until to a gel was obtained. The resultant gel was maintained at 80 °C for 36 h at vacuum drying oven. The precursor gel was then introduced into a muffle furnace and sintered at 1000 °C for 2 h to get target products. MNb_2O_6 (M: Zn, Ni, Co and Mn) sensing materials were prepared with the same method according to above-described procedure, respectively.

The structural properties of the products were characterized with Rigaku wide- angle X-ray diffractometer (D/max rA, using Cu Kα radiation at wave length = 0.1541 nm) in the angular range of 20–80°. Field-emission scanning electron microscopy (FESEM) measurements of surface morphology of the $CdNb_2O_6$-SE materials were performed using a JEOL JSM–7500F microscope with an accelerating voltage of 10 kV. X-ray photoelectron spectroscopy (XPS) measurements were performed on a Thermo ESCALAB250 spectrometer equipped with an Al-Kα ray source. Fourier transform infrared spectroscopy (FTIR) of the $CdNb_2O_6$ sensing electrode material was recorded in the wavenumber range of 1200–400 cm^{-1} with a PE-400 spectrometer at room temperature. A technique of power pellets with KBr at a mass ratio of 1:200 was applied.

2.2. Fabrication and measurement of gas sensor

The sensor was fabricated using the YSZ plate (8 mol% Y_2O_3-doped, 2 mm × 2 mm square, 0.3 mm thickness, provided by Anpeisheng Corp., China). A point-shaped and a narrow stripe-shaped Pt electrode (reference electrode, RE) were formed on two ends of the YSZ plate using a commercial Pt paste (Sino-platinum Metals Co., Ltd.), and sintered at 1000 °C. The various sensing materials obtained were mixed with a minimum quantity of deionized water, respectively. Then, the resultant paste was applied on the point-shaped Pt to form stripe-shaped sensing electrode (SE), and then the device was sintered at 800 °C for 2 h to gain good contact between the sensing electrode and electrolyte. The Pt heater printed on Al_2O_3 substrate was then fixed to the YSZ plate by the inorganic adhesive, which provided the required heating temperature for the sensor. The schematic diagram of the sensor is shown in Fig. 1.

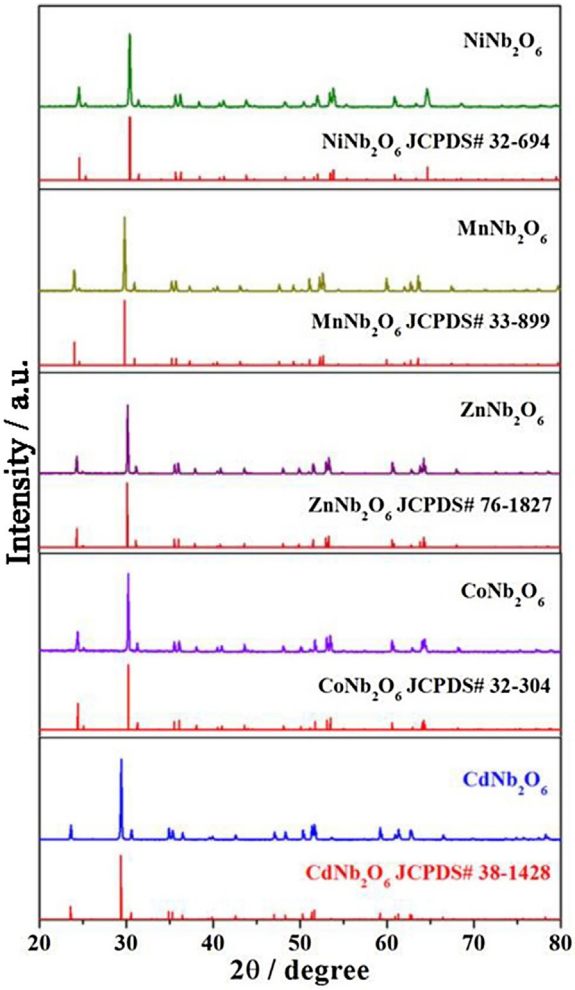

Fig. 2. XRD patterns of MNb_2O_6 (M: Cd, Co, Zn Mn and Ni) composite oxide materials.

The gas sensing characteristics of fabricated sensors were evaluated by a conventional static method. The detailed gas sensing measurement technique as followed: the sensor fabricated was placed in airtight chamber with volume of 1L. Before the measurement, the pure air was filled using an air pump. Then, a certain

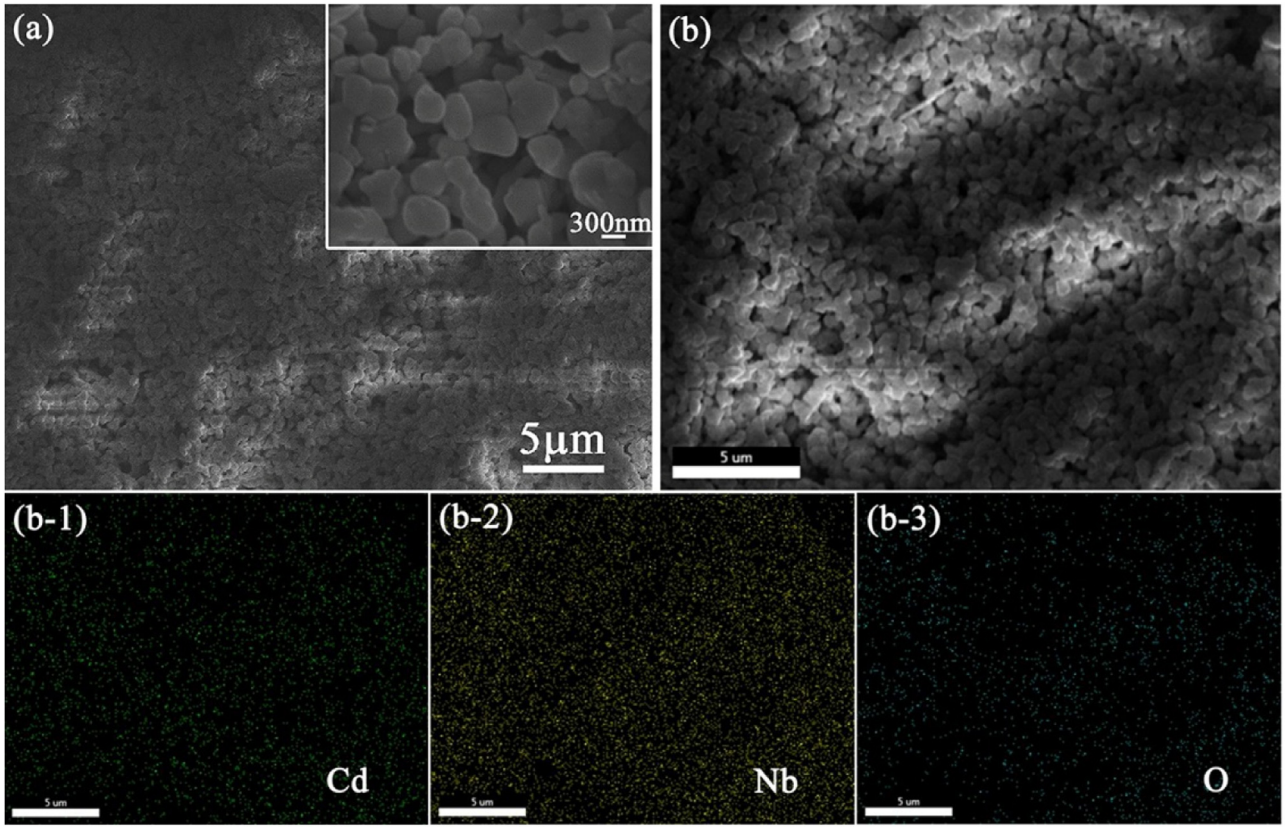

Fig. 3. SEM images of $CdNb_2O_6$-SE material; (b) EDS mapping images for the element of Cd, Nb and O of $CdNb_2O_6$.

amount of acetone or other solvents were injected into the chamber via a special airlock at side of the chamber using a microsyringe and the ventilators in the chamber were working fast to make the test gases distributed uniformly in the chamber. The whole process was controlled by intelligent system and the time it took was less than a second [20,21]. The electric potential difference (V) between the SE and the RE was measured with a digital electrometer (Rigol Technologies, Inc., DM3054, China) when the sensor was exposed to air or sample gas. The results obtained were recorded with a computer connected to the electrometer. The current–voltage (polarization) curves of the sensor were carried out via the potentiodynamic method (CHI650C, Instrument corporation of Shanghai, China) using a two-electrode configuration in the base gas (air) and the different concentrations of acetone gas (2, 5 and 10 ppm) at 600 °C.

3. Results and discussion

To confirm the composition and crystalline phase of synthesized products, the X-ray diffraction (XRD) patterns of columbite type composite oxide materials were measured as shown in Fig. 2. The distinct and sharp diffraction peaks for the prepared composite oxide sensing electrode materials indicate the good crystalline nature. All the XRD peaks for $CdNb_2O_6$, $CoNb_2O_6$, $ZnNb_2O_6$, $MnNb_2O_6$ and $NiNb_2O_6$ could be indexed to orthorhombic columbite structure of $CdNb_2O_6$ (JCPDS#38-1428), $CoNb_2O_6$ (JCPDS#32-304), $ZnNb_2O_6$ (JCPDS#76-1827), $MnNb_2O_6$ (JCPDS#33-899) and $NiNb_2O_6$ (JCPDS#32-694), respectively. No impurity phases were observed from the pattern, which suggests the high purity of material. The morphology of $CdNb_2O_6$ sensing electrode material was characterized by FESEM as presented in Fig. 3. SEM images clearly reveal that $CdNb_2O_6$-SE material shows the loose and porous structure, which is composed of particle with the rough size of approximately 500 nm. Furthermore, Fig. 3(b) displayed EDS mapping images of surface of $CdNb_2O_6$-SE material. For the single columbite phase $CdNb_2O_6$, the elemental mapping measurement further confirms the coexistence and homogeneous dispersion of Cd, Nb and O elements.

XPS measurement was performed to further determine the surface compositions and chemical states of the prepared $CdNb_2O_6$ sensing electrode material. All spectra were calibrated with respect to the binding energy of adventitious C1s peak at 284.7 eV. From the survey spectrum (Fig. 4a), the pearks of Cd, Nb, O and C could be clearly observed in the product. Fig. 4b–d show the high resolution scans of Cd 3d, Nb 3d and O 1s. The Cd 3d spectrum revealed two fitting peaks centered at 411.8 and 404.8 eV, which correspond to the Cd $3d_{3/2}$ and Cd $3d_{5/2}$, respectively, indicating the existence of Cd^{2+} in the $CdNb_2O_6$ material [22]. Fig. 4**c** presents the Nb 3d spectrum and the Nb 3d was composed of two obvious peaks at 209.7 and 206.9 eV, being attributed to Nb $3d_{3/2}$ and Nb $3d_{5/2}$, respectively. The position of the Nb 3d doublet and the binding energy width equal to 2.8 eV between the peak of Nb $3d_{3/2}$ and Nb $3d_{5/2}$ confirmed the Nb^{5+} oxidation state [23]. In Fig. 4d, the O 1 s spectrum was asymmetric and could be fitted into two peaks. The binding energy peak positions at around 531.7 and 530.2 eV could be assigned to chemisorbed oxygen species and typital lattice oxygen in the surface of $CdNb_2O_6$ material, respectively [24]. Additionally, the preliminary information on structure of $CdNb_2O_6$ was also got by IR spectroscopy measurement. Fig. 5 presents the IR spectrum of $CdNb_2O_6$ sensing electrode material. The band with maximum prak at 881 cm^{-1} can be assigned to the stretching vibration of Nb-O in NbO_6 octahedron [25–27]. It is also noteworthy that bands with maxima at 515 and inflection point at 498 cm^{-1} may be assigned to the bending vibrations of O—Nb—O bonds in the NbO_6 octahedron [28]. The bands appearing at 651 and 585 cm^{-1} correspond to the stretching vibrations of Cd—O bonds in the octahedron

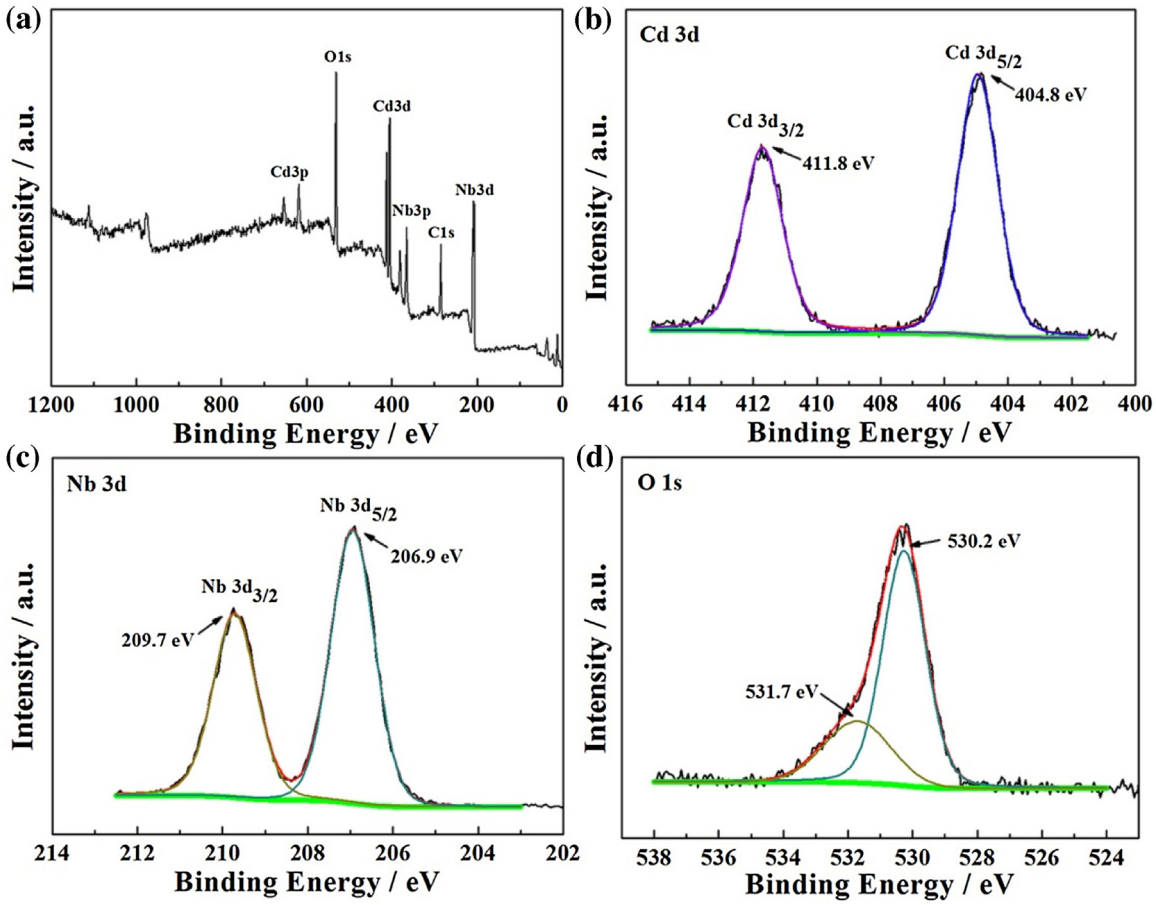

Fig. 4. XPS spectra of $CdNb_2O_6$ composite oxide material (a) survey, (b) Cd 3d, (c) Nb 3d, (d) O 1s.

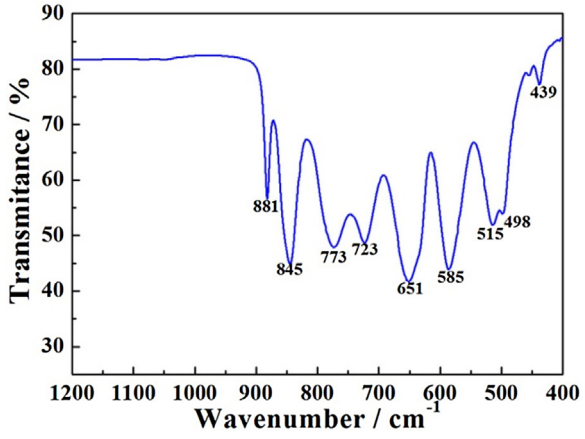

Fig. 5. FT-IR spectrum of $CdNb_2O_6$ composite oxide material.

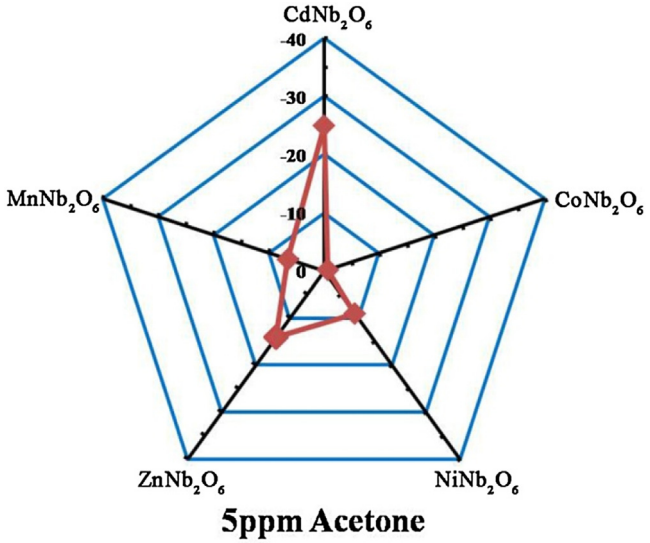

Fig. 6. Response of sensors attached with different sensing electrode materials to 5 ppm acetone at 600 °C.

[29]. The position at 439 cm^{-1} could be assigned to the deformation vibration of the bonds O—Cd—O in CdO_6 polyhedron [30]. The bands of the maxima at 845, 773 and 723 cm^{-1} are interpreted as corresponding to the stretching vibrations of the bridge bonds Cd—O—Nb [31,32].

In order to get the most suitable sensing electrode material for the acetone sensor among the prepared oxides, the responses of sensors using MNb_2O_6-SEs to 5 ppm acetone were measured and corresponding results were shown in Fig. 6. It is clear that the sensor attached with $CdNb_2O_6$-SE displayed the highest response values (−25 mV) to 5 ppm of acetone comparing with the devices utilizing other oxide materials. As a result, the sensing characteristics of the sensor utilizing $CdNb_2O_6$-SE are fully investigated in the following content. The present fabricated device involved the mixed-potential mechanism and could be expressed by the following electrochemical cells:

In air: O_2, $CdNb_2O_6$/YSZ/Pt, O_2

In sample gas: C_3H_6O +O_2, $CdNb_2O_6$/YSZ/Pt, C_3H_6O +O_2

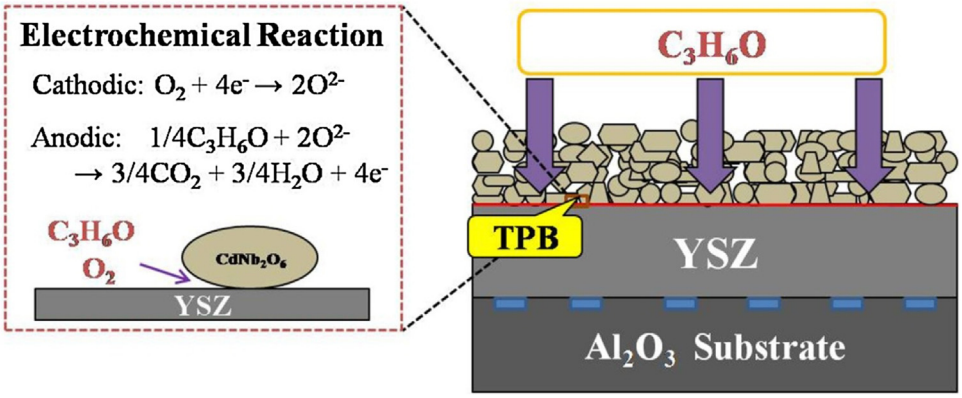

Fig. 7. Schematic view of sensing model for fabricated sensor.

In the presence of sample gas, the cathodic Reaction of O_2 (1) and the anodic Reaction of acetone (2) can proceed simultaneously at the TPB (triple phase boundary, the interface of acetone and $CdNb_2O_6$-SE/YSZ) of SE and form a local cell, as shown in Fig. 7. The mixed potential is achieved when the rates of two electrochemical reactions reach the dynamic equilibrium. The sensing signal of sensor is equal to the potential difference of sensing electrode and reference electrode.

$$\text{Cathodic reaction}: O_2 + 4e^- \rightarrow 2O^{2-} \quad (1)$$

$$\text{Anodic reaction}: 1/4C_3H_6O + 2O^{2-} \rightarrow 3/4CO_2 + 3/4H_2O + 4e^- \quad (2)$$

In the case of present sensor, the mixed potential is strongly dependent on rates of electrochemical Reactions (1) and (2) at TPB. In order to further clarify the reason for the highest response of the sensor utilizing $CdNb_2O_6$-SE and validate the proposed mixed-potential mechanism, the modified polarization curves of the sensor attached with different sensing electrodes in air and 5 ppm acetone and the polarization curves of the sensor utilizing $CdNb_2O_6$-SE in different concentrations of acetone at 600 °C were measured and shown in Fig. 8. The cathodic polarization curve was obtained in air, and the anodic polarization curve was obtained by subtracting in air from in sample gas (different concentration of acetone + air). From the perspective of a mixed-potential model [33,34], the mixed potential is strongly dependent on rates of electrochemical Reactions (1) and (2) at TPB of MNb_2O_6-SE/YSZ/Acetone. A good mixed potential response to acetone can be achieved by one or the combination of the following conditions: an increase in the anodic electrochemical Reaction (2) and a decrease in the cathodic electrochemical Reaction (1). It is obvious that the polarization curve for the anodic reaction of acetone for the device using $CdNb_2O_6$-SE shifts downward to higher current values, compared with others of those sensing electrode materials. This indicates that sensor using $CdNb_2O_6$-SE exhibits the highest electrochemical catalytic activity to anodic Reaction (2) of acetone. In this case, the sensor attached with $CdNb_2O_6$-SE displayed the highest response value to acetone at 600 °C. Additionally, the mixed potential can be estimated from the intersection of the cathodic and anodic polarization curves. Based on the comparison of the mixed potential estimated values and the potential difference values experimentally observed for sensor utilizing $CdNb_2O_6$-SE to different concentrations of acetone at 600 °C, in Table 1. The estimated values are in close proximity to those observed values. Additionally, the estimated and experimentally observed sensitivities of the device to acetone in the concentration range of 1–10 ppm

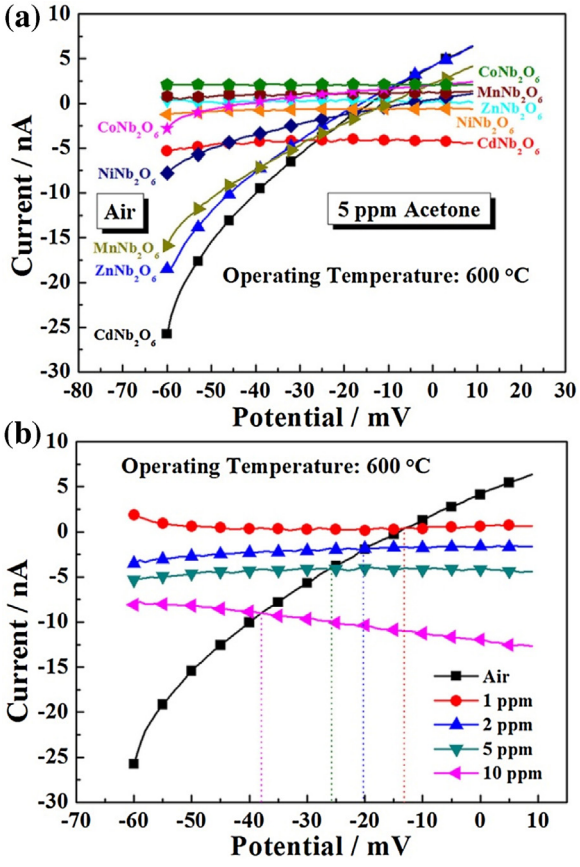

Fig. 8. (a) Polarization curves in air and 5 ppm acetone for the sensors using MNb_2O_6 (M: Cd, Zn, Ni, Co and Mn)-SEs at 600 °C; (b) polarization curves in different concentrations of acetone for the sensor attached with $CdNb_2O_6$-SE at 600 °C.

were extremely close. These coincidences further indicate that the fabricated sensor conforms to the sensing mechanism involving the mixed potential [35–37].

It is well known that the response of the sensor is largely influenced by the operating temperature. Therefore, the responses of the sensor attached with $CdNb_2O_6$-SE towards 5 ppm acetone were investigated as a function of operating temperature. As seen in Fig. 9(a), the response of present sensor to 5 ppm acetone increases initially with the increasing of the operating temperature and reaches a maximum value at 600 °C, and then the response of decrease with further increase of the operating temperature. At low working temperature, the activation energy for electrochemical reaction is deficient, leading to a poor response. With increas-

Table 1
Comparison of the mixed potential estimated and the potential difference value observed for the sensor utilizing $CdNb_2O_6$-SE.

Sensors	Acetone Conc. (ppm)	Mixed potential (estimated) (mV)	Potential difference value (observed) (mV)
$CdNb_2O_6$-SE	1	−13	−10
$CdNb_2O_6$-SE	2	−19.5	−16.5
$CdNb_2O_6$-SE	5	−26	−25
$CdNb_2O_6$-SE	10	−37.5	−32.5
Sensitivity (mV/decade)		−23	−22

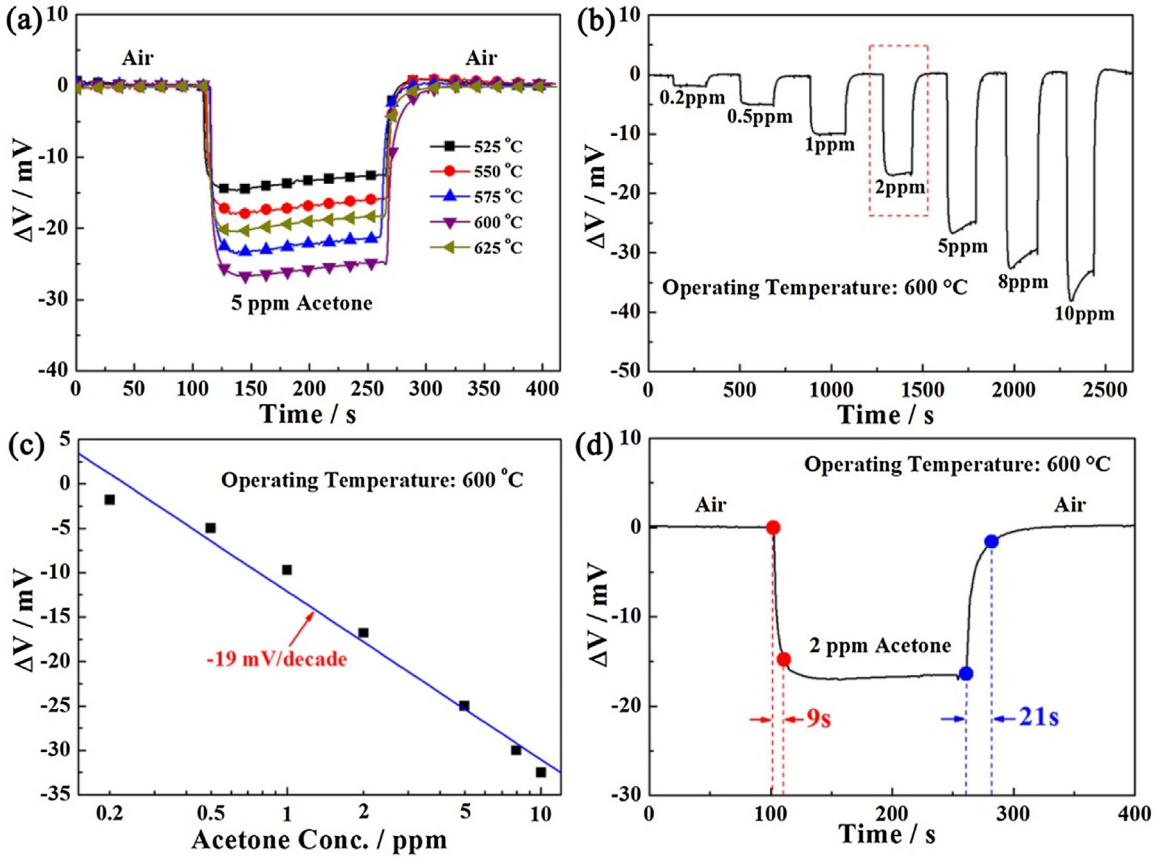

Fig. 9. (a) Response and recovery transients for the sensor using $CdNb_2O_6$-SE to 5 ppm acetone at different operating temperatures; (b) response transients for the sensor attached with $CdNb_2O_6$-SE toward different concentrations of acetone in the range of 0.2–10 ppm at 600 °C; (c) dependence of ΔV for the sensor attached with $CdNb_2O_6$-SE on the acetone concentration at 600 °C; (d) response and recovery times of present sensor to 2 ppm acetone.

ing the working temperature, the electrochemical reaction at TPB will quickly accelerate, leading to improved response. While further increasing the working temperature, the desorption process of acetone proceeds dominant, and cause the amount of acetone adsorbed on the SE to decrease, which lead to deterioration of response at higher temperature. Consequently, the optimal operating temperature for the present sensor was considered to be 600 °C.

The response transients of fabricated sensor attached with $CdNb_2O_6$-SE toward different concentrations of acetone in the range of 0.2–10 ppm was measured at 600 °C and shown in Fig. 9(b). It is apparent that the response increases with the increase of acetone concentration. Note that the sensor exhibits a low detection limit of 200 ppb to acetone. The corresponding response values can reach −2 and −32.5 mV–0.2 and 10 ppm acetone at 600 °C, respectively. Furthermore, the dependence of ΔV for the sensor attached with $CdNb_2O_6$-SE on the acetone concentration in the examined range at 600 °C was shown in Fig. 9(c). ΔV varied almost linear to the logarithm of acetone concentrations in the range of 0.2–10 ppm at 600 °C, which supports mixed potential type model [34,38,39]. The sensitivity of the device is −19 mV/decade. Besides, the present device exhibits fast response and recovery rates in the range of measured concentrations and the typical 90% response and recovery times toward 2 ppm of acetone are 9 and 21 s. As depicted in Fig. 3(a), the loose and porous channels of sensing electrode layer facilitated acetone gas to reach the TPB and participated directly in electrochemical reactions, which shortened the time in the diffusion process. Moreover, according to result of polarization curve, the electrochemical reaction activity at TPB was much higher, and reaction rate was accelerated, which shortened the reaction time of arriving at dynamic equilibrium. Combining these factors together, the sensor displayed rapid response and recovery times. Based on above results, the comparison of the acetone sensing property for the fabricated sensor and those reported previously in literatures is presented in Table 2. Obviously, the present device exhibited better sensing performance to acetone than previously reported devices. Additionally, the effect of different oxygen concentration on acetone sensing performance is investigated. The dependence of ΔV for the sensor utilizing $CdNb_2O_6$-SE to 5 ppm acetone on the logarithm of O_2 concentrations at 600 °C was shown in Fig. 10(a). It can be seen that ΔV was almost positive linear to the logarithm of O_2

Table 2
Comparison of the acetone sensing performances of the present sensor and those of devices reported in literatures.

Material	Acetone Conc. (ppm)	Response (mV)	Sensitivity (mV/decade)	Response Variation/ppm	Low Detection limit (ppm)	Reference
$CdNb_2O_6$	5	−25	−19	5	0.2	Present work
$NiNb_2O_6$	5	−14.5	−13	2.9	0.5	[20]
$Zn_3V_2O_8$	5	−13	−16	2.6	1	[19]
Flower-like WO_3	100	17.4 ($R = R_a/R_g$)	–	0.17	1	[40]
Porous ZnO/$ZnCo_2O_4$	100	7.5 ($R = R_a/R_g$)	–	0.075	10	[41]
ZnO nanorod	5	2.3 ($R = R_a/R_g$)	–	0.46	1	[42]
$ZnFe_2O_4$ hollow microspheres	20	11.3 ($R = R_a/R_g$)	–	0.57	1	[43]
ZnO/$ZnFe_2O_4$ nanosheets	100	16.8 ($R = R_a/R_g$)	–	0.17	5	[44]
$ZnFe_2O_4$ yolk-shell microspheres	20	14 ($R = R_a/R_g$)	–	0.7	0.5	[45]

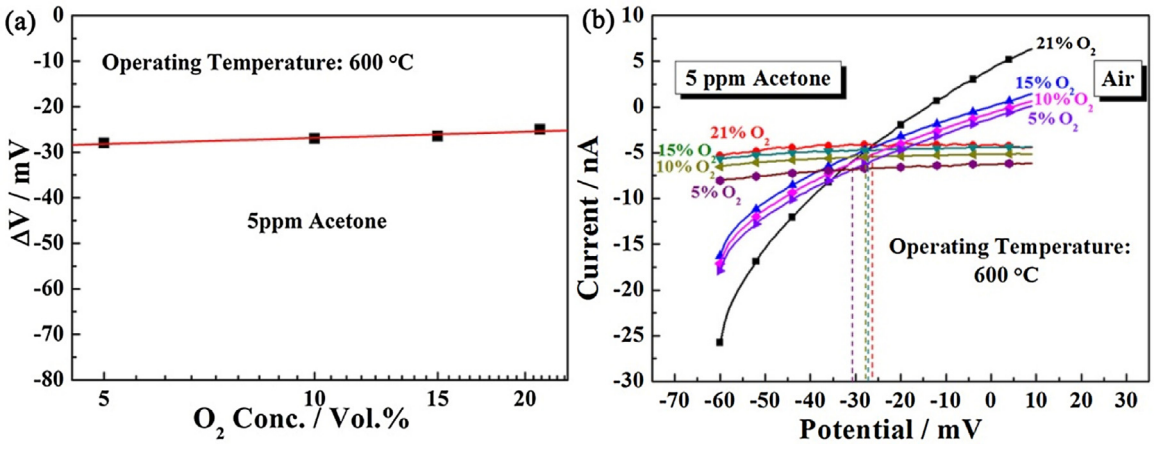

Fig. 10. (a) Dependence of ΔV for the sensor utilizing $CdNb_2O_6$-SE to 5 ppm acetone on the logarithm of O_2 concentrations at 600 °C; (b) Polarization curves of the sensor attached with $CdNb_2O_6$-SE in different concentrations of O_2 at 600 °C.

Table 3
Comparison of the mixed potential estimated and the potential difference value observed for the sensors attached with $CdNb_2O_6$-SE at different concentration of O_2 at 600 °C.

Sensors	Acetone Conc. (ppm)	O_2 Conc. (Vol.%)	Mixed potential (estimated) (mV)	Potential difference value (observed) (mV)
$CdNb_2O_6$-SE	5	5	−30.5	−28
$CdNb_2O_6$-SE	5	10	−28	−27
$CdNb_2O_6$-SE	5	15	−27	−26.5
$CdNb_2O_6$-SE	5	21	−26.5	−25

concentrations in the range of 5–21Vol.% and the response value changed slightly. Meanwhile, the polarization curves of the sensor in different concentrations of O_2 at 600 °C were investigated and exhibited in Fig. 10(b). Based on comparison of mixed potential estimated values and potential difference values experimentally observed for the device fabricated, in Table 3, both values in each case are close to each other. Such results also supported the sensing mechanisms involving the mixed potential.

The V response of mixed potential type sensor fabricated can be explained quantitatively according to Butler-Volmer equation, as has been done before [7,8,34,46]. Each current density for cathodic Reaction (1) and anodic Reaction (2) can be presented by Eqs. (3) and (4), respectively.

$$i_{O_2} = i^0_{O_2} \exp[-4\alpha F(V - V^0_{O_2})/RT] \quad (3)$$

$$i_{Acetone} = i^0_{Acetone} \exp[4\beta F(V - V^0_{Acetone})/RT] \quad (4)$$

Here, V and V^0 are the electrode potential and the equilibrium electrode potential; i^0 the exchange current density; α and β represent transfer coefficient; F, R and T are the Faraday constant, gas constant and temperature, respectively. i^0 is hypothesised to follow kinetic Eqs. (5) and (6).

$$i^0_{O_2} = -B_1 C^m_{O_2} \quad (5)$$

$$i^0_{Acetone} = B_2 C^n_{Acetone} \quad (6)$$

Where B_1, B_2, m, and n are constants, C_{O_2} and $C_{Acetone}$ represent the concentration of O_2 and Acetone, respectively. The mixed potential V_M is defined as the electrode potential at which the current densities of acetone and oxygen addition are equal to zero. Additionally, based on above-obtained Eqs. (3)–(6), V_M can be expressed by Eq. (7):

$$V_M = V_0 + mA \ln C_{O_2} - nA \ln C_{Acetone} \quad (7)$$

Here,

$$V_0 = \frac{RT}{(4\alpha + 4\beta)F} \ln \frac{B_1}{B_2} + \frac{2\alpha V^0_{O_2} + 2\beta V^0_{Acetone}}{2\alpha + 2\beta} \quad (8)$$

$$A = \frac{RT}{(4\alpha + 4\beta)F} \quad (9)$$

When O_2 concentration is fixed, Eq. (7) is simplified to the following equation:

$$V_M = V_0 - nA \ln C_{Acetone} \quad (10)$$

Thus, the linear relationship between V_M and the logarithm of acetone concentration displays negative slope under the fixed concentration value of O_2, which has been observed experimentally

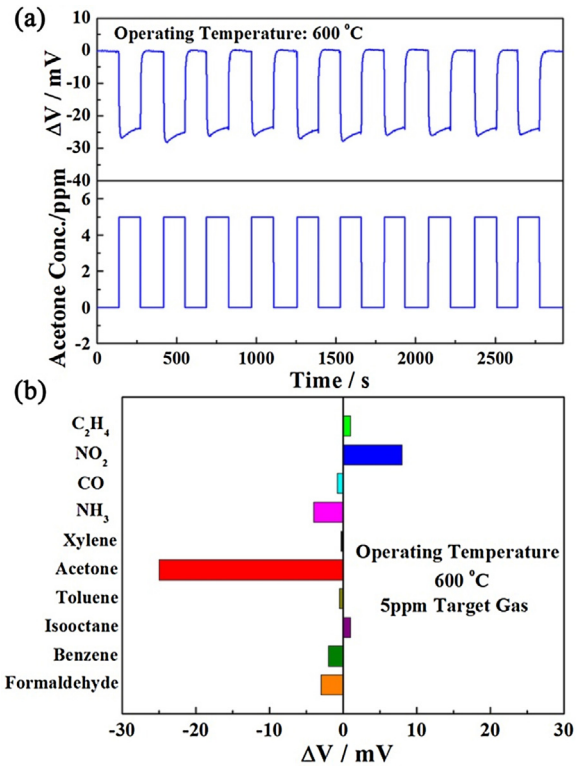

Fig. 11. (a) Continuous response and recovery transients to 5 ppm acetone for the sensor attached with $CdNb_2O_6$-SE at 600 °C; (b) cross-sensitivities for the sensor attached with $CdNb_2O_6$-SE to 5 ppm of various gases at 600 °C.

in Fig. 9(c) very well. With regard to the fixed concentration of acetone, on the other hand, V_M should positively linearly with the logarithm of O_2 concentration. Fig. 10 indicates that the linear correlations have positive slope with increasing oxygen concentration under fixed concentration of acetone, in agreement with theory (+mA) from Eq. (7). Such theoretical analysis further demonstrated that the present sensor conformed to the mixed potential mechanism.

Fig. 11(a) shows the continuous response-recovery transients of the present sensor to 5 ppm acetone at 600 °C. Obviously, the responses of the present device to 5 ppm acetone had little fluctuation in the examined ten-time cycles, which indicated that the sensor exhibited good repeatability. The selectivity for the sensor attached with $CdNb_2O_6$-SE to various gases at 600 °C, such as toluene, benzene, NO_2 and NH_3, etc was evaluated and shown in Fig. 11(b). It is obvious that the fabricated sensor exhibited relative high responses to 5 ppm of acetone comparing with those of other interfering gases. This result illuminates that the present device possessed good selectivity to acetone. From the perspective of practical application, the sensitivity of sensor to a target gas should not be affected by the change of relative humidity during use. Accordingly, the responses for the sensor attached with $CdNb_2O_6$-SE to 10 ppm acetone in the relative humidity (RH) range of 15–98% at 600 °C are measured and results obtained are demonstrated in Fig. 12(a,b). The effect of RH on the response of the sensor fabricated is small in the examined humidity range and the change amplitudes to 10 ppm acetone in the RH of 20%, 60% and 98% are −1.5%, −18.5% and −23.1%. As another vital factor for evaluating sensing performance, the stability of the sensor utilizing $CdNb_2O_6$-SE was investigated by continuous working at high temperature of 600 °C during interval of 30 days. The responses of the sensor to 2, 5

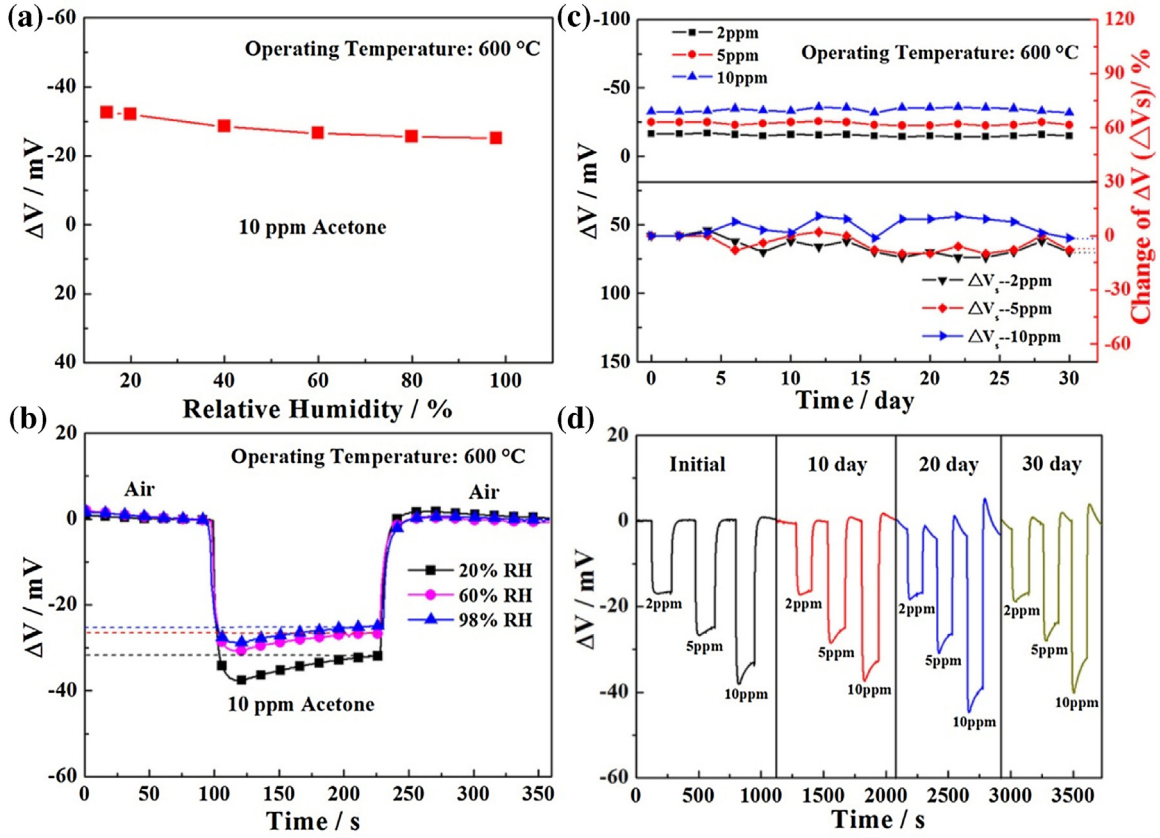

Fig. 12. (a) Response of the sensor attached with $CdNb_2O_6$-SE to 10 ppm acetone at 600 °C under different relative humidity; (b) response and recovery transients for the sensor using $CdNb_2O_6$-SE to 10 ppm acetone under 20%, 60% and 98% relative humidity at 600 °C; (c) Long-term stability to 2, 5 and 10 ppm acetone for the sensor attached with $CdNb_2O_6$-SE at 600 °C; (d) response and recovery transients for the sensor using $CdNb_2O_6$-SE to 2, 5 and 10 ppm acetone on the initial, 10th, 20th and 30th day.

and 10 ppm acetone were measured every other day and obtained results are recorded in Fig. 12(c,d). The change amplitude of the ΔV for the sensor attached with $CdNb_2O_6$-SE changed slightly to 2, 5 and 10 ppm acetone during 30 days measurement period. In order to further illustrate quantitatively the change amplitude of the ΔV with time, the change of the ΔV ($\triangle V_s$) for the sensor is given by $\triangle V_s = [(\Delta V_n - \Delta V_0)/\Delta V_0 \times 100\%]$, where ΔV_n and ΔV_0 denote the ΔV of the sensor on the n and initial day, respectively. The quantitative results showed that the $\triangle V_s$ for the sensor to 2, 5 and 10 ppm acetone on the 30th day were −9.1%, −8.0% and −1.5%, respectively. In order to better understand the changes in the process of aging, the response and recovery transients for the sensor using $CdNb_2O_6$-SE to 2, 5 and 10 ppm acetone on the initial, 10th, 20th and 30th day are shown in Fig. 12(d). The result indicated that four response and recovery transients of the present device to 2, 5 and 10 ppm acetone remain relatively better consistency. Therefore, the present fabricated sensors also showed good stability during the measurement period. The sensing performances of fabricated sensor in sensitivity, low detection limit, wet-resistance and stability showed that the sensor developed has a good potential application prospect in acetone detection.

4. Conclusion

In this work, YSZ-based mixed potential type gas sensors using MNb_2O_6 (M: Cd, Zn, Ni, Mn and Co) columbite-type composite oxide as SEs were developed and used for detection of sub-ppm acetone at 600 °C. Among the different oxide sensing electrode materials, $CdNb_2O_6$ was found to the most suitable SE for acetone sensor. Results showed that the sensor attached with $CdNb_2O_6$-SE displayed low detection limit of 200 ppb acetone and had potential application in monitoring sub-ppm acetone. Additionally, the present sensor also exhibited high response, rapid response and recovery times, good sensitivity, repeatability, selectivity, relative better moisture resistance and stability in 30 days measurement periods at high-temperature-aging of 600 °C to acetone. Consequently, the present device is one of promising candidate for detecting acetone in the aspect of diabetes diagnosis based on excellent sensing performances.

Acknowledgements

This work is supported by the National Nature Science Foundation of China (Nos. 61134010, 61327804, 61374218, 61473132, 61533021 and 61520106003), Program for Chang Jiang Scholars and Innovative Research Team in University (No. IRT13018) and National High-Tech Research and Development Program of China (863 Program, No. 2014AA06A505), Application and Basic Research of Jilin Province (2013010 2010JC).

References

[1] J. Wolfsdorf, N. Glaser, M. Sperling, Diabetic ketoacidosis in infants, children, and adolescents: a consensus statement from the American Diabetes Association, Diabetes Care 143 (2009) 111–118.
[2] J.-B. Yu, H.-G. Byun, M.-S. So, J.-S. Huh, Analysis of diabetic patient's breath with conducting polymer sensor array, Sens. Actuators B: Chem. 108 (2005) 305–308.
[3] C. Deng, J. Zhang, X. Yu, W. Zhang, X. Zhang, Determination of acetone in human breath by gas chromatography–mass spectrometry and solid-phase microextraction with on-fiber derivatization, J. Chromatogr. B. 810 (2004) 269–275.
[4] K. Kao, M. Hsu, Y. Chang, S. Gwo, J. Yeh, A sub-ppm acetone gas sensor for diabetes detection using 10 nm thick ultrathin InN FETs, Sensors 12 (2012) 7157–7168.
[5] M. Righettoni, A. Tricoli, S. Pratsinis, Si: WO_3 sensors for highly selective detection of acetone for easy diagnosis of diabetes by breath analysis, Anal. Chem. 82 (2010) 3581–3587.
[6] N. Miura, H. Kurosawa, M. Hasei, G. Lu, N. Yamazoe, Stabilized zirconia-based sensor using oxide electrode for detection of NO_x in high-temperature combustion-exhausts, Solid State Ionics 86-88 (1996) 1069–1073.
[7] G. Lu, N. Miura, N. Yamazoe, High-temperature hydrogen sensor based on stabilized zirconia and a metal oxide electrode, Sens. Actuators B: Chem. 35-36 (1996) 130–135.
[8] N. Miura, T. Raisen, G. Lu, N. Yamazoe, Highly selective CO sensor using stabilized zirconia and a couple of oxide electrodes, Sens. Actuators B: Chem. 47 (1998) 84–91.
[9] Y. Fujio, V. Plashnitsa, P. Elumalai, N. Miura, Stabilization of sensing performance for mixed-potential-type zirconia-based hydrocarbon sensor, Talanta 85 (2011) 575–581.
[10] R. Moos, K. Sahner, M. Fleischer, U. Guth, N. Barsan, U. Weimar, Solid state gas sensor research in Germany –a status report, Sensors 9 (2009) 4323–4365.
[11] Y. Li, X. Li, Z. Tang, Z. Tang, J. Yu, J. Wang, Hydrogen sensing of the mixed-potential-type $MnWO_4$/YSZ/Pt sensor, Sens. Actuators B: Chem. 206 (2015) 176–180.
[12] N. Miura, G. Lu, N. Yamazoe, High-temperature potentiometric/amperometric NO_x sensors combining stabilized zirconia with mixed-metal oxide electrode, Sens. Actuators B: Chem. 52 (1998) 169–178.
[13] G. Lu, N. Miura, N. Yamazoe, A high temperature amperometric NO sensor based on stabilized zirconia and $CdCr_2O_4$ electrode, J. Appl. Electrochem. 28 (1998) 1009–1011.
[14] V. Plashnitsa, T. Ueda, P. Elumalai, N. Miura, NO_2 sensing performances of planar sensor using stabilized zirconia and thin-NiO sensing electrode, Sens. Actuators B: Chem. 130 (2008) 231–239.
[15] Y. Fujio, V. Plashnitsa, M. Breedon, N. Miura, Construction of sensitive and selective zirconia-based CO sensors using $ZnCr_2O_4$-based sensing electrodes, Langmuir 28 (2012) 1638–1645.
[16] L. Zhou, Q. Yuan, X. Li, J. Xu, F. Xia, J. Xiao, The effects of sintering temperature of $(La_{0.8}Sr_{0.2})_2FeMnO_{6-\delta}$ on the NO_2 sensing property for YSZ-based potentiometric sensor, Sens. Actuators B: Chem. 206 (2015) 311–318.
[17] X. Zhang, H. Kohler, M. Schwotzer, U. Guth, Mixed-potential gas sensor with PtAu-8YSZ sensing electrode: electric potential difference measurements at isothermal and thermo-cyclic operation, Sens. Actuators B: Chem. 217 (2015) 107–112.
[18] F. Liu, Y. Guan, R. Sun, X. Liang, P. Sun, F. Liu, G. Lu, Mixed potential type acetone sensor using stabilized zirconia and $M_3V_2O_8$ (M: Zn Co and Ni) sensing electrode, Sens. Actuators B: Chem. 221 (2015) 673–680.
[19] F. Liu, X. Yang, B. Wang, Y. Guan, X. Liang, P. Sun, G. Lu, High performance mixed potential type acetone sensor based on stabilized zirconia and $NiNb_2O_6$ sensing electrode, Sens. Actuators B: Chem. 229 (2016) 200–208.
[20] Q. Diao, C. Yin, Y. Guan, X. Liang, S. Wang, Y. Liu, Y. Hu, H. Chen, G. Lu, The effects of sintering temperature of $MnCr_2O_4$ nanocomposite on the NO_2 sensing property for YSZ-based potentiometric sensor, Sens. Actuators B: Chem. 177 (2013) 397–403.
[21] C. Wang, X. Cheng, X. Zhou, P. Sun, X. Hu, K. Shimanoe, G. Lu, N. Yamazoe, Hierarchical α-Fe_2O_3/NiO composites with a hollow structure for a gas sensor, ACS Appl. Mater. Interfaces 6 (2014) 12031–12037.
[22] J. Moulder, W. Stickle, K. Bomben, Handbook of X-ray Photoelectron Spectroscopy:a Reference Book of Standard Spectra for Indentification and Interpretation of XPS Data, Perkin-Elmer Corporation, Physical Electronics Division, USA, 1992.
[23] M. Mazur, M. Szymańska, D. Kaczmarek, M. Kalisz, D. Wojcieszak, J. Domaradzki, F. Placido, Determination of optical and mechanical properties of Nb_2O_5 thin films for solar cells application, Appl. Surf. Sci. 301 (2014) 63–69.
[24] S. Lam, J. Sin, I. Satoshi, A. Abdullah, A. Mohamed, Enhanced sunlight photocatalytic performance over Nb_2O_5/ZnO nanorod composites and the mechanism study, Appl. Catal. A 471 (2014) 126–135.
[25] A. Pawlicka, M. Atik, M. Aegerter, Synthesis of multicolor Nb_2O_5 coatings for electrochromic devices, Thin Solid Films 301 (1997) 236–241.
[26] P. Tabero, Synthesis and properties of $FeNb_{11}O_{29}$, Ceram. Silik. 49 (2005) 126–131.
[27] S. Pauline, N. Rajendran, Biomimetic novel nanoporous niobium oxide coating for orthopaedic applications, Appl. Surf. Sci. 290 (2005) 448–457.
[28] P. Tabero, A. Tabero, P. Szilágyi, Z. Homonnay, The investigations of phases with general formula $M_2FeV_3O_{11}$, where M = Mg Co, Ni, Zn by IR and Mössbauer spectroscopy, J. Phys. Chem. Solids 68 (2007) 1087–1090.
[29] K. Anandhan, R. Kumar, Synthesis, FTIR UV–vis and photoluminescence characterizations of triethanolamine passivated CdO nanostructures, Spectrochim. Acta Part A 149 (2015) 476–480.
[30] E. Filipek, M. Piz, A new compound in the Nb-V-Sb-O system and its physicochemical characteristic, J. Alloys Compd. 661 (2016) 141–147.
[31] X. Zhang, R. Frech, Spectroscopic investigation of $Li_{1+x}V_3O_8$, Electrochim. Acta 42 (1977) 475–482.
[32] R. Yuvakkumar, S. Hong, Structural phase transitions in niobium oxide nanocrystals, Phase Transitions 88 (2015) 897–906.
[33] N. Miura, G. Lu, N. Yamazoe, Progress in mixed-potential type devices based on solid electrolyte for sensing redox gases, Solid State Ionics 136–137 (2000) 533–542.
[34] N. Miura, T. Sato, S. Anggraini, H. Ikeda, S. Zhuiykov, A review of mixed-potential type zirconia-based gas sensors, Ionics 20 (2014) 901–925.
[35] J. Wang, P. Elumalai, D. Terada, M. Hasei, N. Miura, Mixed-potential-type zirconia-based NO_x sensor using Rh-loaded NiO sensing electrode operating at high temperatures, Solid State Ionics 177 (2006) 2305–2311.

[36] T. Sato, V. Plashnitsa, M. Utiyama, N. Miura, Potentiometric YSZ-based sensor using NiO sensing electrode aiming at detection of volatile organic compounds (VOCs) in air environment, Electrochem. Commun. 12 (2010) 524–526.
[37] X. Liang, S. Yang, J. Li, H. Zhang, Q. Diao, W. Zhao, G. Lu, Mixed-potential- type zirconia-based NO_2 sensor with high-performance three-phase boundary, Sens. Actuators B: Chem. 158 (2011) 1–8.
[38] N. Miura, S. Zhuiykov, T. Ono, M. Hasei, N. Yamazoe, Mixed potential type sensor using stabilized zirconia and $ZnFe_2O_4$ sensing electrode for NO_x detection at high temperature, Sens. Actuators B: Chem. 83 (2002) 222–229.
[39] G. Lu, Q. Diao, C. Yin, S. Yang, Y. Guan, X. Cheng, X. Liang, High performance mixed-potential type NO_x sensor based on stabilized zirconia and oxide electrode, Solid State Ionics 262 (2014) 292–297.
[40] J. Huang, X. Xu, C. Gu, M. Yang, M. Yang, J. Liu, Large-scale synthesis of hydrated tungsten oxide 3D architectures by a simple chemical solution route and their gas-sensing properties, J. Mater. Chem. 21 (2011) 13283–13289.
[41] X. Zhou, W. Feng, C. Wang, X. Hu, X. Li, P. Sun, K. Shimanoe, N. Yanazoe, G. Lu, Porous $ZnO/ZnCr_2O_4$ hollow spheres: synthesis, characterization, and applications in gas sensing, J. Mater. Chem. A 2 (2014) 17683–17690.
[42] Y. Zeng, T. Zhang, M. Yuan, M. Kang, G. Lu, R. Wang, H. Fan, Y. He, H. Yang, Growth and selective acetone detection based on ZnO nanorod arrays, Sens. Actuators B: Chem. 143 (2009) 93–98.
[43] X. Zhou, X. Li, H. Sun, P. Sun, X. Liang, F. Liu, X. Hu, G. Lu, Nanosheet-assembled $ZnFe_2O_4$ hollow microspheres for high-sensitive acetone sensor, ACS Appl. Mater. Interfaces 7 (2015) 15414–15421.
[44] X. Li, C. Wang, H. Guo, P. Sun, F. Liu, X. Liang, G. Lu, Double-shell architectures of $ZnFe_2O_4$ nanosheets on ZnO hollow spheres for high- performance gas sensors, ACS Appl. Mater. Interfaces 7 (2015) 17811–17818.
[45] X. Zhou, B. Wang, H. Sun, C. Wang, P. Sun, X. Li, X. Hu, G. Lu, Template-free synthesis of hierarchical $ZnFe_2O_4$ yolk-shell microspheres for high-sensitivity acetone sensors, Nanoscale 8 (2016) 5446–5453.
[46] G. Lu, N. Miura, N. Yamazoe, High-temperature sensors for NO and NO_2 based on stabilized zirconia and spinel-type oxide electrodes, J. Mater. Chem. 7 (1997) 1445–1449.

Biographies

Fangmeng Liu received his B.S. degree in 2009 from College of Chemistry, Liaocheng University and M.S. degree in 2012 from Northeast Forestry University in China. Currently he is studying for his Ph.D. degree in College of Electronic Science and Engineering, Jilin University, China.

Bin Wang received the B.Eng. degree in department of electronic science and technology in 2015. He is currently studying for his M.E. Sci. degree in College of Electronic Science and Engineering, Jilin University, China.

Xue Yang received the B.Eng. degree in department of electronic science and technology in 2015. She is currently studying for his M.E. Sci. degree in College of Electronic Science and Engineering, Jilin University, China.

Xishuang Liang received the B. Eng. degree in Department of Electronic Science and Technology in 2004. He received his Doctor's degree in College of Electronic Science and Engineering at Jilin University in 2009. Now he is an associate professor of Jilin University, China. His current research is solid electrolyte gas sensor.

Peng Sun received his PhD degree from the Electronics Science and Engineering department, Jilin University, China in 2014. Now, he is engaged in the synthesis and characterization of the semiconducting functional materials and gas sensors.

Xiaohong Chuai is an associate professor and works in Department of Electrical Engineering, Jilin University, China. Her research interests are focused on sensor materials and devices.

Yuan Gao received her PhD degree from Department of Analytical Chemistry at Jilin University in 2012. Now she is a lecturer in Jilin University, China. Her current research is focus on the preparation and application of graphene oxide and semiconductor oxide, especial in gas sensor and biosensor.

Fengmin Liu received the BE degree in Department of Electronic Science and Technology in 2000. She received his Doctor's degree in College of Electronic Science and Engineering at Jilin University in 2005. Now she is a professor in Jilin University, China. Her current research is preparation and application of semiconductor oxide, especial in gas sensor and solar cell.

Geyu Lu received the B.Sci. degree in electronic sciences in 1985 and the M.S. degree in 1988 from Jilin University in China and the Dr. Eng. degree in 1998 from Kyushu University in Japan. Now he is a professor of Jilin University, China. His current research interests include the development of chemical sensors and the application of the function materials.